

Received: 2018.01.31

Accepted: 2018.09.11

Published: 2019.01.19

# <sup>18</sup>F-Deoxyglucose (<sup>18</sup>F-FDG) Positron Emission Tomography/Computed Tomography (PET/CT) Monitoring of Dynamic Growth Characteristics of Walker-256 Tumor Models in 3 Different Locations in Rats

Authors' Contribution:  
Study Design A  
Data Collection B  
Statistical Analysis C  
Data Interpretation D  
Manuscript Preparation E  
Literature Search F  
Funds Collection G

ABCDEF 1,2,3

ABCD 1,2,3

DE 2,4

AD 1,2,3,5

AG 1,2,3

Panli Li\*  
Qiufang Liu\*  
Xiuying Wang  
Gang Huang  
Shaoli Song

1 Department of Nuclear Medicine, Ren Ji Hospital, School of Medicine, Shanghai Jiao Tong University, Shanghai, P.R. China  
2 Shanghai Jiao Tong University-University of Sydney (SJTU-USYD) Joint Research Alliance for Translational Medicine, Shanghai Jiao Tong University, Shanghai, P.R. China  
3 Institute of Clinical Nuclear Medicine, Ren Ji Hospital, School of Medicine, Shanghai Jiao Tong University, Shanghai, P.R. China  
4 Biomedical and Multimedia Information Technology Research Group, School of Information Technologies, University of Sydney, Sydney, Australia  
5 Shanghai University of Medicine and Health Sciences, Shanghai, P.R. China

\* Panli Li and Qiufang Liu contributed equally to the writing of this article

Corresponding Author: Shaoli Song, e-mail: shaoli-song@163.com

Source of support: This work was funded by the National Natural Science Foundation of China (Grant No. 81771861,81471708) and the Shanghai Jiao Tong University Medical Engineering Cross Research Fund (No. YG2016MS55)

**Background:** We explored the ideal method of establishing subcutaneous, breast, and liver tumor models using the same Walker-256 cells, and investigated the dynamic growth characteristics using <sup>18</sup>F-deoxyglucose (<sup>18</sup>F-FDG) positron emission tomography/computed tomography (PET/CT), which provides basic information for choosing an experimental animal model.


**Material/Methods:** We established tumor models in 3 locations (subcutaneous, breast, and liver) in W256 Sprague-Dawley rats. <sup>18</sup>F-FDG PET/CT imaging was performed from 6 days to 18 days after injecting the cells subcutaneously. Tumor volume of interest (VOI), maximum standard uptake value (SUV<sub>max</sub>), and average standard uptake value (SUV<sub>avg</sub>) were obtained from the image. The difference of the growth characteristics in tumor volume and SUVs among the 3 groups were compared. Histopathology of the tumors was also analyzed.

**Results:** The tumors in subcutaneous location grew fastest, followed by tumors located in the breast, and tumors in the liver grew slowest. Significant differences in tumor VOI ( $p=0.01$ ) were observed. <sup>18</sup>F-FDG uptake of the subcutaneous and breast tumors increased until day 10 and then decreased subsequently. <sup>18</sup>F-FDG uptake of the liver tumor reached a peak at day 10, and necrosis peaked at day 12. The histopathology analysis results indicated that the necrosis was mainly located in the center of tumors while the viable tissues were located on the periphery. Similarly, CD 31 and Ki-67 were mainly expressed on the tumor periphery.

**Conclusions:** Subcutaneous, breast, and liver tumor models were easy to establish using Walker-256 cells. They showed fast growth and high uptake of <sup>18</sup>F-FDG. These kinds of tumor models were optimal in evaluating anti-tumor efficacy by <sup>18</sup>F-FDG PET/CT, but it may be essential to determine the best time-points at which to use it.

MeSH Keywords: **Fluorodeoxyglucose F18 • Immunohistochemistry • Models, Animal • Nuclear Medicine • Positron-Emission Tomography**

Full-text PDF: <https://www.medscimonit.com/abstract/index/idArt/909286>

 2411

 —

 5

 20



## Background

Cancer is still a worldwide threat to human health. Breast cancer is the leading cause of cancer death among females worldwide and liver cancer is the sixth most common cancer and the third leading cause of cancer-related mortality worldwide [1]. Although surgery, radiotherapy, and chemotherapy are widely used clinically, recurrence or metastasis still happens and leads to poor prognosis. Therefore, more research is needed on suitable animal tumor models to validate the efficacy of radiotherapy and chemotherapy in basic research.

The Walker-256 rat cell line is the pure strain of epithelial cells from this tumor discovered in 1928 by Walker in the breast of a pregnant rat as a mammary carcinosarcoma [2] and been widely used for its high tumorigenicity and invasive growth pattern. Many researches also used Walker-256 cells to induce a bone metastasis model because it can simulate the expansion and invasion of malignant tumors. It has been used to establish a variety of tumor models with Sprague-Dawley (SD) or Wistar rats for oncology research, such as breast cancer [3], skeletal metastases [4] and liver cancer [5–8].

Clinically, early treatment response evaluation can help to adjust the therapeutic schedule. Magnetic resonance imaging (MRI) and computed tomography (CT) can only reflect the tumor size and burden. Currently, positron emission tomography/computed tomography (PET/CT) is a commonly used non-invasive method that provides information on the biological functionality of the tumor based on the uptake of a radiolabeled tracer [9–11]. Changes in the uptake tracer changing after treatment can be used for early response evaluation and to predict the treatment outcome. In particular, glucose analogue <sup>18</sup>F-deoxyglucose (<sup>18</sup>F-FDG) PET/CT has been established as an important tool for the study of tumorigenesis, tumor development, metastasis, and therapeutic effects. Apart from glucose consumption, the tracer <sup>18</sup>F-fluorothymidine (<sup>18</sup>F-FLT) is a thymidine analogue, which reflects changes in tumor cell proliferative activity. However, different drugs inhibit tumor growth via various mechanisms at different cell cycle phases, and combination chemotherapy is often used clinically to treat patients with tumors, which leads to complicated changes in tumor DNA synthesis. In this situation, <sup>18</sup>F-FLT uptake cannot adequately reflect tumor cell proliferation [12,13]. Therefore, <sup>18</sup>F-FDG PET/CT is the most universal means of detection, but there are few published studies about <sup>18</sup>F-FDG PET/CT in the existing models.

Thus, we established subcutaneous, breast, and liver tumor models in rats using the same Walker-256 cells. Consecutive <sup>18</sup>F-FDG PET/CT scans were conducted to observe the dynamic characteristics of tumor growth *in vivo*. We non-invasively analyzed the metabolic characteristics and built a dynamic growing

database of rat tumor models, which can provide the basis for choosing the best animal model for use in experiments.

## Material and Methods

### Animals and cell line

All the animal care and experimental procedures were conducted in accordance with the guidelines of the Ren Ji Institutional Animal Care and Animal Ethics Committee [14]. Female Sprague-Dawley rats (200–250 g) were purchased from the Ren Ji Hospital Experimental Animal Center, China. Rats were kept under specific pathogen-free conditions at the Laboratory Animal Center. The Walker-256 cell line was obtained from the Laboratory of Translational Medicine of the Jiangsu Province Academy of Traditional Chinese Medicine. The cells were maintained in RPMI-1640 medium (Gibco) supplemented with 10% fetal bovine serum (FBS) (Gibco) and 1% penicillin–streptomycin (Gibco) and were incubated at 37°C with 5% CO<sub>2</sub> and 100% humidity.

### Establishment of tumor models

A total of 15 Sprague-Dawley rats (200–250 g) were used to establish subcutaneous tumor (female rats, n = 5), breast tumor (female rats, n = 5) and liver tumor (female rats, n = 5) models Walker-256 cells. Each rat received a subcutaneous injection of Walker-256 cells (0.1 mL, 1×10<sup>7</sup>) in the right front flank. Walker-256/B cells (0.1 mL, 1×10<sup>7</sup>) were injected into the left second mammary fat pads of each rat for the breast tumor model. For the transplanted liver tumor model, the inoculation was performed as follows: Walker-256 cells (0.1 mL, 1×10<sup>7</sup>) were first injected subcutaneously into a donor rat. When the tumor diameter reached 6–8 mm, the donor rat was anesthetized with 10% chloral hydrate (3 mL/Kg) and then the tumor was resected and minced into small cubes about 1 mm<sup>3</sup>. The recipient rats were also anesthetized and a 1.5–2 cm long straight lateral rectus incision was made, and the right hepatic lobe was exteriorized on a sterile compress. Then, a tumor block (1 mm<sup>3</sup>) was embedded in the liver lobe of each recipient rat using a handmade tumor conveyer [7,8]. After the conveyer was withdrawn, tissue adhesive (3M Vetbond Tissue Adhesive PN) was used to prevent bleeding. Finally, the incision was closed with suture.

### <sup>18</sup>F-FDG micro-PET/CT imaging

All animals were fasted 6–8 h before they underwent <sup>18</sup>F-FDG PET/CT. Tumor-bearing rats were anesthetized with isoflurane (2% in oxygen) and placed in prone position. <sup>18</sup>F-FDG (37 MBq/0.2 mL) was administrated into the tail vein of each rat. One hour later, a 30-min scan was performed. Rats were

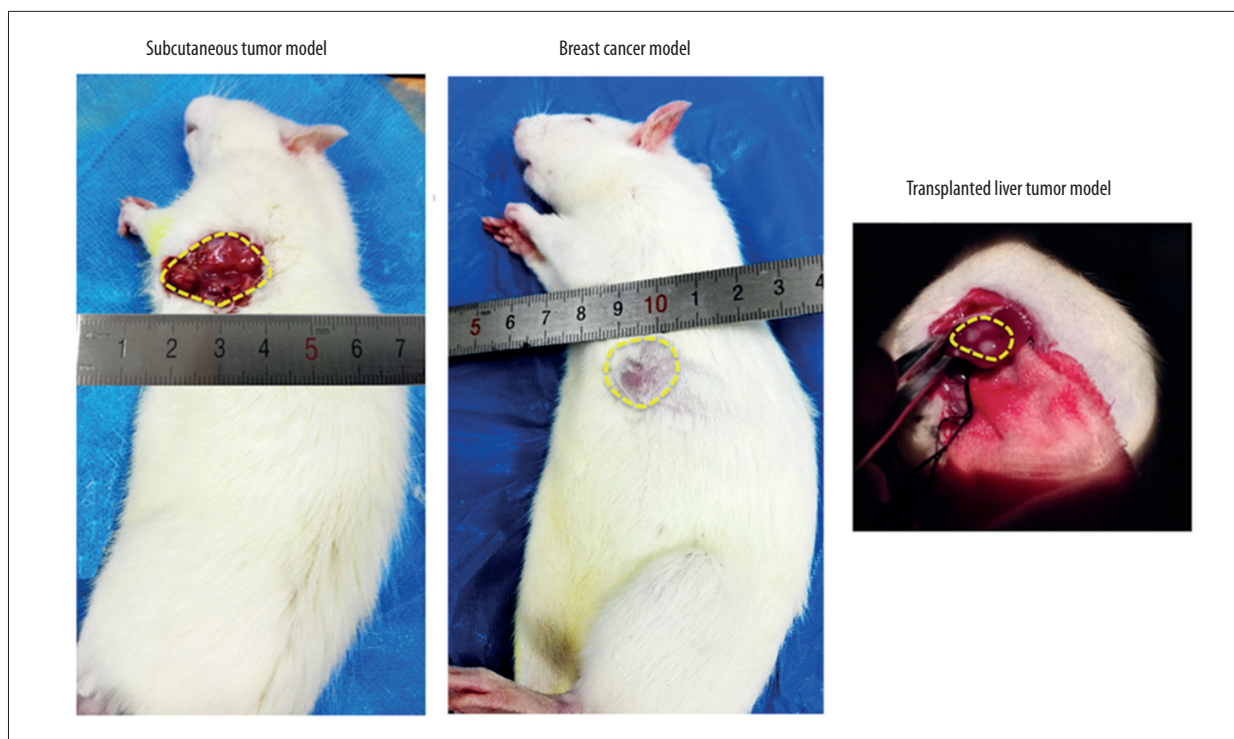


**Figure 1.** Representative photographs of the 3 different location tumor models in subcutaneous, breast, and transplanted liver tumor, respectively, on day 16 or day 18 after inoculation. Yellow circle, tumor.

maintained under anesthesia with 2% isoflurane during the scanning. <sup>18</sup>F-FDG micro-PET/CT imaging (Super Nova® PET/CT, Pingseng, China) was performed, which has a PET spatial resolution of approximately 0.6 mm and a CT voxel size of 0.29 mm. The CT parameters were: x-ray voltage, 60 KV; anode current, and 450 uA. PET images were reconstructed with the ordered-subsets expectation maximization algorithm using 16 subsets and 4 iterations. To estimate the tumor volume of interest, the region of interest covering the tumor was assessed using the 3D segmentation on the PET through Avatar 1.2 software (Pingseng, China). Then, the 3D tumor VOI (VOI<sub>41</sub>) based on 3D isocontour at 41% of the SUV<sub>max</sub> [15], maximum standardized uptake values (SUV<sub>max</sub>), and average standardized uptake values (SUV<sub>avg</sub>) were measured.

<sup>18</sup>F-FDG PET/CT scans were performed at day 6, day 7, day 8, day 10, day 12, day 14, and day 16 after injection into tumors located subcutaneously and in the breast. For transplanted liver tumors, <sup>18</sup>F-FDG PET/CT scans were performed at day 8, day 9, day 10, day 12, day 14, day 16, and day 18 after inoculation.

**Histology analysis**

Rats were sacrificed and tumors of each rat were collected on day 16 or day 18 after micro-PET/CT imaging. Tumor tissues were snap-frozen with an optimum-cutting-temperature compound (Sakura, USA) and sectioned into 3 consecutive

5-mm slices. One slice was stained with hematoxylin-eosin (H&E) and one slice was stained with anti-active Ki-67 polyclonal antibodies according to the manufacturer’s protocol (Novus, USA). Another slice was immunohistochemically stained used anti-CD31 monoclonal antibody to visualize the blood vessels [16]. The remaining slide was stained with terminal TUNEL (Yeasen, China). The cell nuclei were counterstained with 4',6-diamidino-2-phenylindole (DAPI, Sigma) [17]. TUNEL-stained slides were visualized under a fluorescence microscope (Zeiss Axio Observer.Z1).

**Statistics analysis**

Group variation is described as the mean ± standard deviation. The one-way analysis of variance (ANOVA) followed by LSD post hoc test for multiple comparisons was used to compare the differences in tumor VOI and SUVs among the 3 groups (IBM SPSS statistics 22.0, IBM, USA).

**Results**

**Tumor formation and general condition**

None of the animals died during inoculation, and successful tumor growth was observed in the postoperative period (Figure 1). For subcutaneous and breast tumor models, tumors

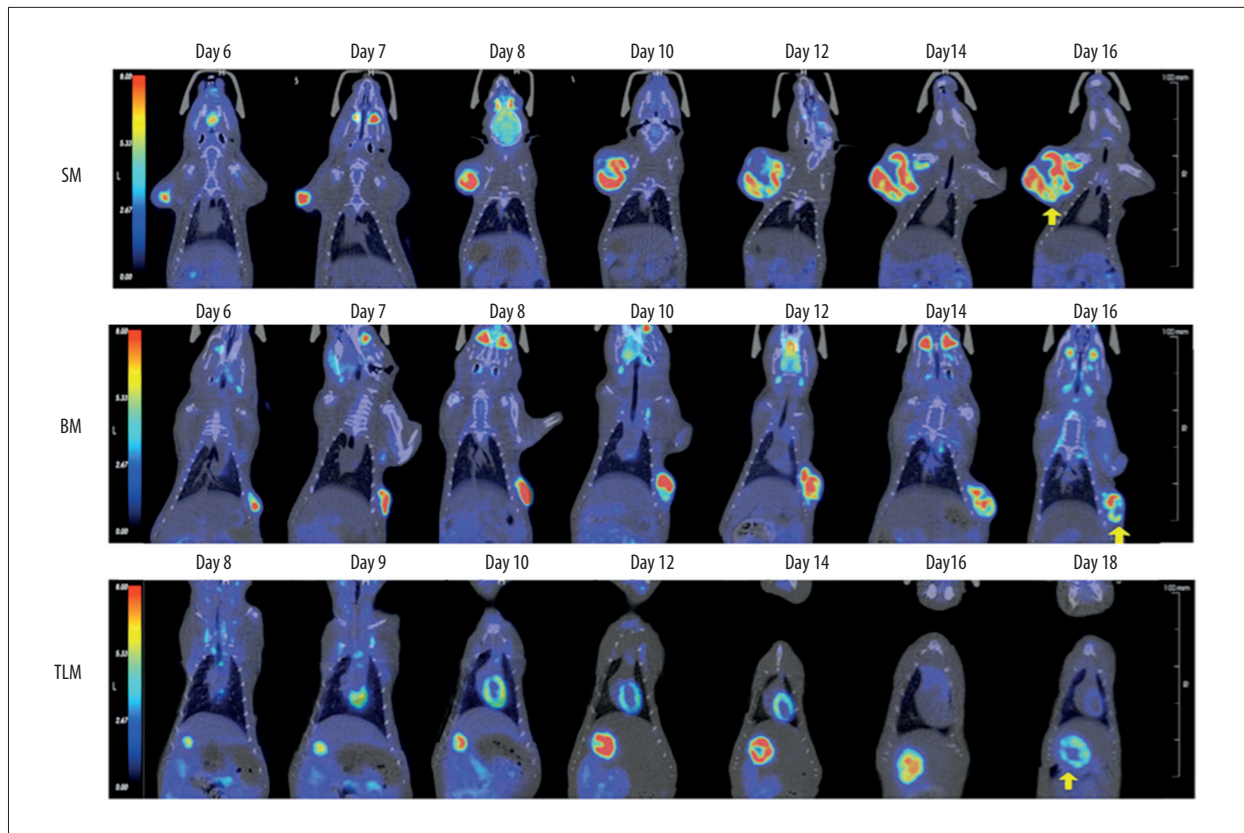


**Figure 2.** Representative <sup>18</sup>F-FDG micro-PET/CT images of the 3 different tumor location models (subcutaneous, breast, and transplanted liver tumor) at different time-points. Arrows indicate tumors.

were visible on day 5 after injection of Walker-256 cells. The liver tumors were detected by <sup>18</sup>F-FDG micro-PET/CT imaging on day 8 after inoculation, and the tumors grew locally in the liver as a solitary nodule. Therefore, the tumor formation rates of the 3 different tumor models were all up to 100%. During the first 10 days, there were no obvious changes in diet or activities of rats. Subsequently, the rats showed relative less activity, uneven fur, and less energy.

### <sup>18</sup>F-FDG micro-PET/CT imaging

Representative <sup>18</sup>F-FDG PET/CT images showed the growth changes of tumors (Figure 2). For tumor in subcutaneous and breast tissue, we found that the uptake of <sup>18</sup>F-FDG continued to increase until day 12, then necrosis began to develop in the central regions of tumors, while the peripheral tumor tissues exhibited high <sup>18</sup>F-FDG uptake. Low <sup>18</sup>F-FDG uptake areas occurred on day 14 after inoculation in the liver tumor model. The SUV<sub>max</sub> value of the subcutaneous model increased from 8.15±0.34 (day 5) to 12.38±0.66 (day 10) and then showed an obvious decline to 8.32±0.21 until day 16. For the breast tumor model, the SUV<sub>max</sub> value climbed to 12.45±0.81 on day 10 and decreased to 8.54±0.46 (day 16). In the liver model, SUV<sub>max</sub> value showed a remarkable increasing trend from day

8 to day 14 and peaked at 9.97±0.24 on day 14, after which it decreased to 6.84±0.92 on day 18. The SUV<sub>max</sub> value of tumors in subcutaneous and breast models had a significant difference compared to the liver model (*p*<0.01). However, we observed no significant differences between subcutaneous and breast tumor models until day 10 (*p*>0.05) (Figure 3A).

The average standard uptake value (SUV<sub>avg</sub>) value peaked at 6.83±0.41 at day 8 and then decreased at subsequent observation timepoints (Figure 3B). For breast tumors, SUV<sub>avg</sub> value climbed to 7.10±0.26 on day 8 and decreased during follow-up (Figure 3B). The SUV<sub>avg</sub> value had no significant differences between tumors in subcutaneous and breast models (*t*=0.90, *p*=0.37). For the liver tumor model, compared with SUV<sub>max</sub> value, the maximum of SUV<sub>avg</sub> value (6.30±0.41) was observed on day 12.

Tumor VOI changes of the 3 tumor location models are shown in Figure 3C. The subcutaneous tumors grew fastest, followed by breast tumors, and the liver tumors grew slowest (*p*=0.01). The subcutaneous tumor VOI increased from the minimal volume of 89.00±5.61 mm<sup>3</sup> (day 6) to the maximal volume of 1116.93±86.56 mm<sup>3</sup> (day 12). The minimal breast tumor VOI on day 6 was more than 9 times smaller than the maximal size

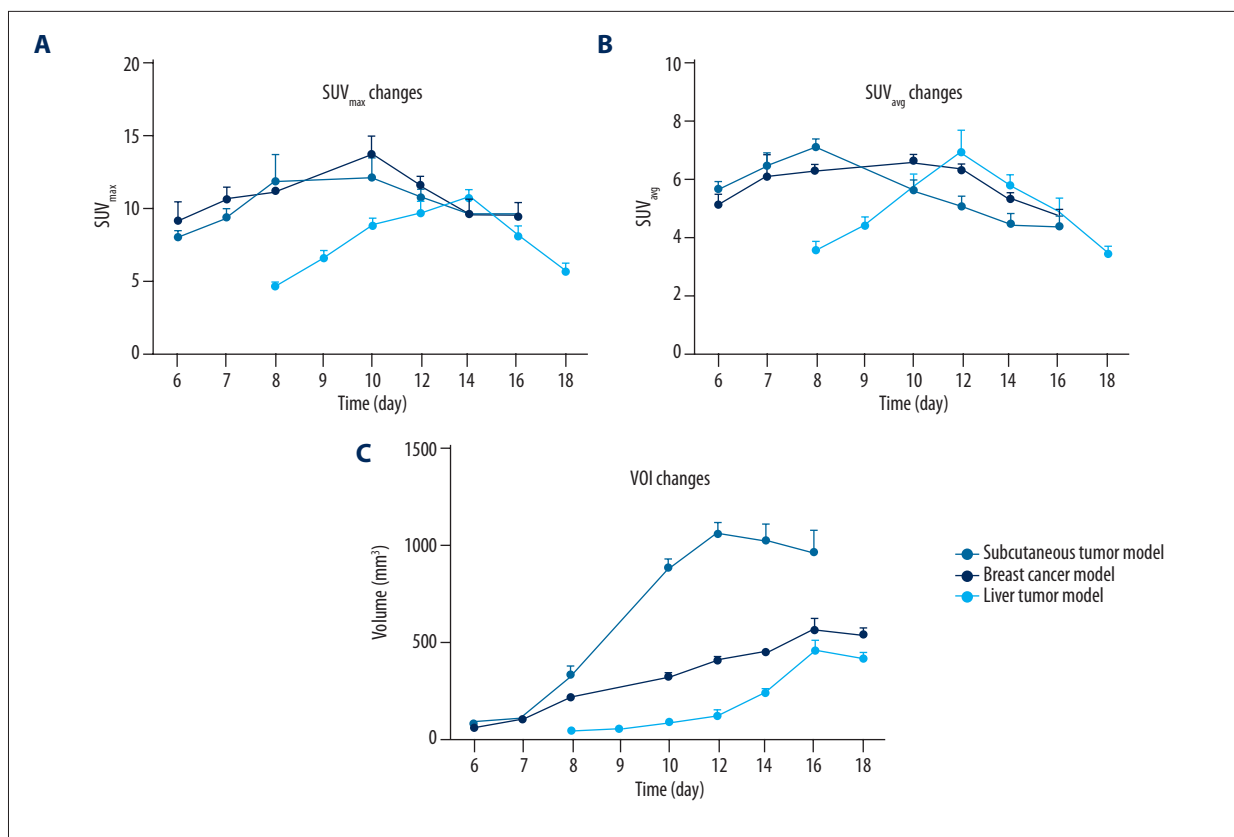


**Figure 3.** (A) The curves of tumor SUV<sub>max</sub> of tumors in subcutaneous, breast, and liver model at different time-points. (B) The curves of tumor SUV<sub>avg</sub> of subcutaneous, breast, and liver tumor model at different time-points. (C) The curves of tumor volume of interest in subcutaneous, breast, and liver tumor model at different time-points. A significant tumor volume of interest difference was observed among the 3 different tumor models.

on day 16 ( $61.83 \pm 5.84 \text{ mm}^3$  vs.  $569.98 \pm 44.83 \text{ mm}^3$ ). Similarly, the liver tumor VOI also showed a continuous upward trend until day 16, rising to  $479.10 \pm 41.70 \text{ mm}^3$ , then the tumor VOI level decrease to  $426.70 \pm 16.62 \text{ mm}^3$  on day 18 ( $p=0.03$ ).

**Histology analysis**

Representative microphotographs of tumors and adjacent normal tissue from rats are shown in Figure 4. The subcutaneous tumors had extensive necrosis and the nodule consisted of few viable tumor cells, fibroblasts, histiocytes, and lymphoplasmacytes. The viable tumor cells showed a solid growth pattern with a vague nesting formation and the nuclei were large and darkly stained. For the breast tumors, we found that the tumor mass was localized in the breast tissue and small necrotic areas were scattered throughout the tumor. Moreover, the tumor cells demonstrated obviously enlarged nuclei and prominent nucleoli, which had infiltrated mammary ductal tissues. The liver tumors had normal liver tissues and revealed degenerative and necrotic changes, and a small focus of tumor nests was found in the periphery of the tumor.

Representative images Figure 5 show the results of immunohistochemical staining for Ki-67, CD 31, and TUNEL. The viable tumor cells presented a high expression of Ki-67, and there was extensive expression of CD 31 in the periphery of the tumors, indicating a relatively high microvessel density. Similarly, TUNEL-positive apoptotic cells were scattered in the tumors in all 3 tumor models.

**Discussion**

In this study, we used the Walker-256 cell line to establish subcutaneous, breast, and liver tumor metastasis models in SD rats. We found that the Walker-256 tumor model has advantages of high tumor formation rate, short experimental period, and simple operation. Compared with nude mice, SD rats have a similar architecture of hemodynamics and immune system to humans. Therefore, when compared to humans, there was little difference in invasiveness, angiogenesis, metastasis, drug delivery, and sensitivity to therapeutic agents [18,19].

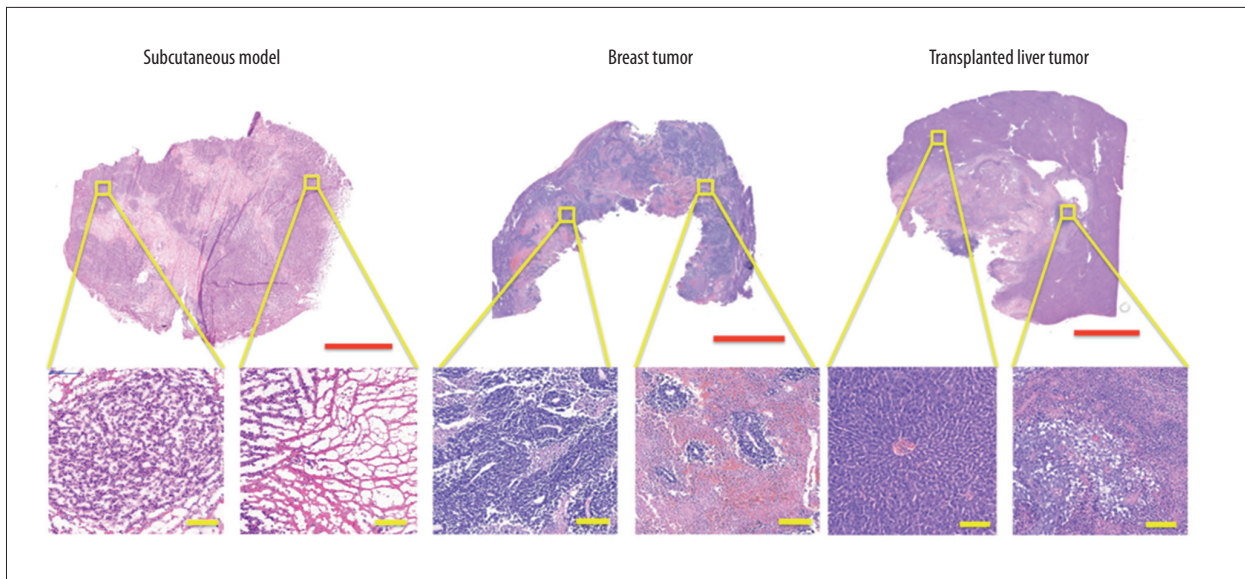


**Figure 4.** H&E staining of subcutaneous tumor, breast tumor, and transplanted liver tumor on day 16 or day 18 after inoculations. Bar in red, 5 mm. Bar in yellow, 100  $\mu$ m.

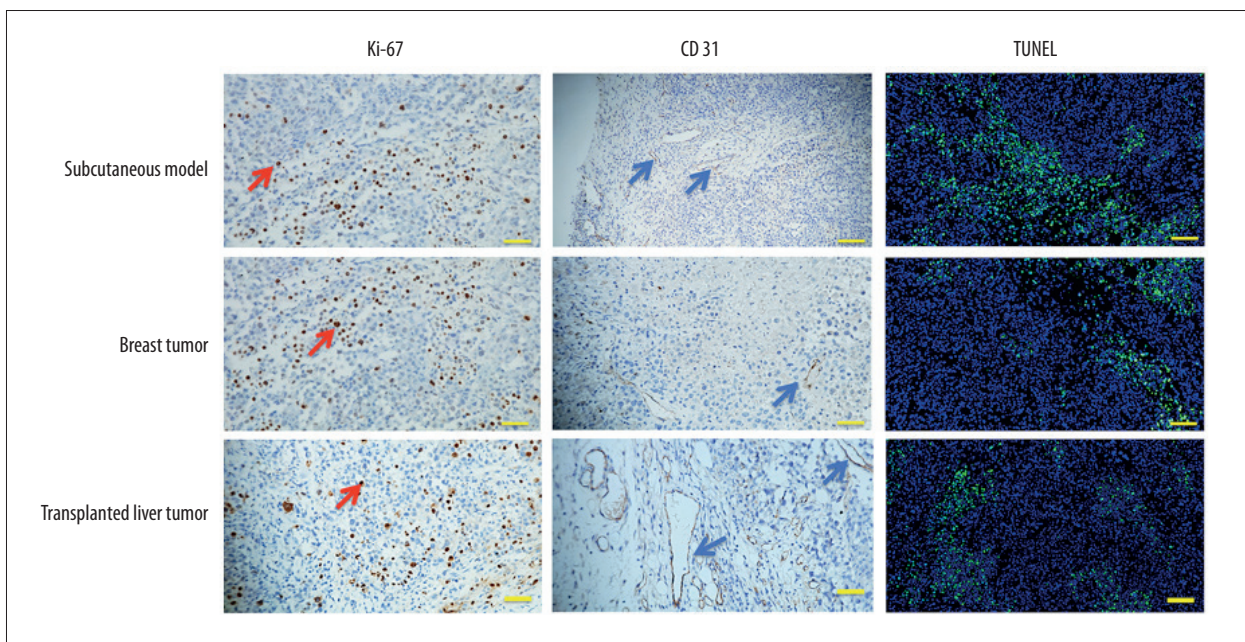


**Figure 5.** Ki-67, TUNEL, and CD 31 staining of subcutaneous tumor, breast tumor, and transplanted liver tumor on day 16 or day 18 after inoculations. Red arrow, cells overexpressing Ki-67. Blue arrow, tumor blood vessels expressing CD 31. Green, TUNEL-positive apoptotic cells. Blue, 4',6-diamidino-2-phenylindole (DAPI)-stained nuclei. Bar in yellow, 100  $\mu$ m.

In our study, we demonstrated several growth characteristics using the  $^{18}\text{F}$ -FDG PET/CT imaging of these 3 different metastasis tumor models established with Walker-256 cells. Firstly, the results revealed that the tumors in the subcutaneous model grew fastest and had the largest tumor volume. The subcutaneous tumor diameter unexpectedly grew to more than 2 cm at the end of the experiment, probably because the Walker-256 cells were injected in the

subcutaneous axillary area, providing larger growth space and better vascularization.

We found that  $\text{SUV}_{\text{max}}$  continued to increase until day 12 in the tumors in the subcutaneous and breast cancer models, but it continued to increase until day 14 in the liver model. There was no significant difference in  $\text{SUV}_{\text{max}}$  between tumors in the subcutaneous and breast models; however, both of them had

a higher SUV<sub>max</sub> than in the liver model. Our results show that the evaluation of anti-cancer treatments should be no later than day 12 because spontaneous necrosis may affect the assessment. The diminution of the SUV<sub>mean</sub> value was linked to the partial volume artifact (mixture of necrosis and viable tumor). Spontaneous necrosis in early period had little influence on the SUV<sub>max</sub> value. In clinical practice, SUV<sub>max</sub> is the main indicator of tumor glycometabolism and predictor of prognosis. It is important to realize that the spontaneous decrease of SUV<sub>max</sub> and SUV<sub>mean</sub> can influence the therapeutic evaluation. Therefore, when performing experiments, it is important to select the best duration of therapy, the optimal detection index, and the correct comparison to the control group.

In addition, we successfully established liver transplanted tumor. Traditionally, liver tumor models have been established by injecting tumor cells using a needle. However, this method has certain problems: a) low inoculation rate, and b) inevitable tumor dissemination, allowing the tumor to spill from the puncture channel [20]. To overcome these difficulties, we embedded a small tumor cube (1 mm<sup>3</sup>) into liver tissues rather than injecting tumor cells, and tissue adhesive was also used to control hemorrhage and peritoneal dissemination of tumor tissue. As a result, we found that the tumor growth was fast and tumor size at each point exhibits only a small variation,

which is crucial in evaluating the efficacy of an anti-tumor therapy. Moreover, the spontaneous necrosis is mainly due to the insufficient growth of tumor support tissue. HE staining showed that after necrosis, the tumor cells ruptured and the nuclear structure disappeared; there were large pieces of red dye found, but little lymphocytic infiltration. The results of anti-CD31 staining in our study suggest that Walker-256 transplanted liver tumors are hypervascular, similar to human hepatocellular carcinoma. This characteristic provides a basis for preclinical research on locoregional therapies of liver cancer.

## Conclusions

In this study, we successfully established 3 different tumor models (subcutaneous, breast, and liver) with Walker-256 cells in rats. The tumor models showed a high uptake of <sup>18</sup>F-FDG and fast growth, indicating that these tumor models are appropriate for the study of <sup>18</sup>F-FDG PET/CT used to evaluate anti-tumor efficacy.

## Conflict of interest

None.

## References:

- Jemal A, Bray F, Center MM et al: Global cancer statistics. *Cancer J Clin*, 2011; 61: 69–90
- Simpkins H, Lehman JM, Mazurkiewicz JE, Davis BH: A morphological and phenotypic analysis of Walker 256 cells. *Cancer Res*, 1991; 51: 1334–38
- Gao M, Zhang D, Jin Q et al: Combretastatin-A4 phosphate improves the distribution and antitumor efficacy of albumin-bound paclitaxel in W256 breast carcinoma model. *Oncotarget*, 2016; 7: 58133–41
- Badraoui R, Rebai T: Effect of malignant ascites on antioxidative potency of two tumoral cells-induced bone metastases: Walker 256/B and MatLyLu. *Exp Toxicol Pathol*, 2012; 64: 65–68
- Li X, Feng GS, Zheng CS et al: Influence of transarterial chemoembolization on angiogenesis and expression of vascular endothelial growth factor and basic fibroblast growth factor in rat with Walker-256 transplanted hepatoma: An experimental study. *World J Gastroenterol*, 2003; 9: 2445–49
- Gao L, Zhang J, Ma T et al: Improved therapeutic outcomes of thermal ablation on rat orthotopic liver allograft sarcoma models by radioiodinated hypericin induced necrosis targeted radiotherapy. *Oncotarget*, 2016; 7: 51450–61
- Liu Q, Qian Y, Li P et al: The combined therapeutic effects of <sup>131</sup>Iodine-labeled multifunctional copper sulfide-loaded microspheres in treating breast cancer. *Acta Pharm Sin B*, 2018; 8: 371–80
- Liu Q, Chen F, Hou L et al: Nanocarrier-mediated chemo-immuno therapy arrested cancer progression and induced tumor dormancy in desmoplastic melanoma. *ACS Nano*, 2018
- Barrington SF, Johnson PWM: <sup>18</sup>F-FDG PET/CT in lymphoma: Has imaging-directed personalized medicine become a reality? *J Nucl Med*, 2017; 58: 1539–44
- Kaira K, Higuchi T, Naruse I et al: Metabolic activity by <sup>18</sup>F-FDG-PET/CT is predictive of early response after nivolumab in previously treated NSCLC. *Eur J Nucl Med Mol Imaging*, 2018; 45(1): 56–66
- Kim YI, Kim YJ, Paeng JC et al: Prediction of breast cancer recurrence using lymph node metabolic and volumetric parameters from <sup>18</sup>F-FDG PET/CT in operable triple-negative breast cancer. *Eur J Nucl Med Mol Imaging*, 2017; 44(11): 1787–95
- Xu W, Yu S, Xin J, Guo Q: <sup>18</sup>F-FLT and <sup>18</sup>F-FDG PET-CT imaging in the evaluation of early therapeutic effects of chemotherapy on Walker 256 tumor-bearing rats. *Exp Ther Med*, 2016; 12: 4154–58
- Jensen MM, Erichsen KD, Johnbeck CB et al: [<sup>18</sup>F]FDG and [<sup>18</sup>F]FLT positron emission tomography imaging following treatment with belinostat in human ovary cancer xenografts in mice. *BMC Cancer*, 2013; 13: 168
- Workman P, Aboagye EO, Balkwill F et al: Guidelines for the welfare and use of animals in cancer research. *Br J Cancer*, 2010; 102: 1555–77
- Boellaard R, Delgado-Bolton R, Oyen WJ et al: FDG PET/CT: EANM procedure guidelines for tumour imaging: version 2.0. *Eur J Nucl Med Mol Imaging*, 2015; 42: 328–54
- CD 31: marker of angiogenesis and a prognostic factor in adult soft tissue sarcomas. *Expert Rev Mol Diagn*, 2002; 2: 526
- Gonzalez JC, Vazquez FJ, Rodriguez Lobato E et al: Determination of apoptosis in actinic prurigo by TUNEL technique. *Photodermatol Photoimmunol Photomed*, 2015; 31: 115–17
- Céspedes MV, Casanova I, Parrero M, Mangués R: Mouse models in oncogenesis and cancer therapy. *Clin Transl Oncol*, 2006; 8: 318–29
- Kerbel RS: Human tumor xenografts as predictive preclinical models for anticancer drug activity in humans: Better than commonly perceived but they can be improved. *Cancer Biol Ther*, 2003; 2: S134–39
- Chen JH, Lin YC, Huang YS et al: Induction of VX2 carcinoma in rabbit liver: comparison of two inoculation methods. *Lab Anim*, 2004; 38: 79–84